Front. Environ. Sci. Eng. 2023, 17(2): 15
https://doi.org/10.1007/s11783-023-1615-2

RESEARCH ARTICLE

Effect of ambient polycyclic aromatic hydrocarbons and nicotine on the structure of $A\beta_{42}$ protein

Samal Kaumbekova[1], Mehdi Amouei Torkmahalleh[1], Naoya Sakaguchi[2], Masakazu Umezawa[2], Dhawal Shah (✉)[1]

1 Department of Chemical and Materials Engineering, School of Engineering and Digital Sciences, Nazarbayev University, Kabanbay Batyr 53, Nur-Sultan, 010000, Kazakhstan
2 Department of Materials Science and Technology, Faculty of Advanced Engineering, Tokyo University of Science, 6-3-1 Niijuku, Katsushika, Tokyo 125-8585, Japan

HIGHLIGHTS

- B[a]P, nicotine and phenanthrene molecules altered the secondary structure of $A\beta_{42}$.
- β-content of the peptide was significantly enhanced in the presence of the PAHs.
- Nicotine made stable cluster with $A\beta_{42}$ peptide via hydrogen bonds.
- Phenanthrene due to its small size, interfered with the $A\beta_{42}$ monomer more strongly.

GRAPHIC ABSTRACT

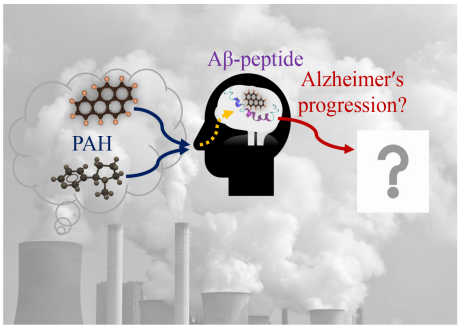

ARTICLE INFO

Article history:
Received 24 March 2022
Revised 16 June 2022
Accepted 3 July 2022
Available online 31 August 2022

Keywords:
Polycyclic aromatic hydrocarbons
Nicotine
toxicology
$A\beta_{42}$ peptide
Alzheimer's disease
Molecular dynamics simulations
Environmental pollution

ABSTRACT

Recent studies have correlated the chronic impact of ambient environmental pollutants like polycyclic aromatic hydrocarbons (PAHs) with the progression of neurodegenerative disorders, either by using statistical data from various cities, or via tracking biomarkers during *in-vivo* experiments. Among different neurodegenerative disorders, PAHs are known to cause increased risk for Alzheimer's disease, related to the development of amyloid beta (Aβ) peptide oligomers. However, the complex molecular interactions between peptide monomers and organic pollutants remains obscured. In this work, we performed an atomistic molecular dynamics study via GROMACS to investigate the structure of $A\beta_{42}$ peptide monomer in the presence of benzo[a]pyrene, nicotine, and phenanthrene. Interestingly the results revealed strong hydrophobic, and hydrogen-bond based interactions between Aβ peptides and these environmental pollutants that resulted in the formation of stable intermolecular clusters. The strong interactions affected the secondary structure of the $A\beta_{42}$ peptide in the presence of the organic pollutants, with almost 50 % decrease in the α-helix and 2 %–10 % increase in the β-sheets of the peptide. Overall, the undergoing changes in the secondary structure of the peptide monomer in the presence of the pollutants under the study indicates an enhanced formation of Aβ peptide oligomers, and consequent progression of Alzheimer's disease.

1 Introduction

The concern about environmental pollutants was exhibited recently with advanced prediction modeling of their enhanced concentrations (Shang et al., 2021; Zhang et al., 2021). Environmental pollution contributes to the progression of neurogenerative disorders through direct or indirect molecular pathways (Heusinkveld et al., 2016; Hahad et al., 2020). Recent studies by Calderón-Garcidueñas et al. (2016) highlighted the connection between air pollutants and AD biomarkers among children of Mexico City. Among different air pollutants, ultrafine particles (UFPs), known as $PM_{0.1}$ (particulate matter with the aerodynamic size of less than 0.1 μm),

✉ Corresponding author
E-mail: dhawal.shah@nu.edu.kz

due to their small size have rapid translocation to the brain through the blood brain barrier or the olfactory route (Oberdörster et al., 2004; Heusinkveld et al., 2016). Furthermore, $PM_{0.1}$ may adsorb a significant amount of toxic organic compounds given their high surface area (Kwon et al., 2020). Considering that citizens spend most of their time in indoor environments (Klepeis et al., 2001), recent studies on human subjects showed that exposure to indoor UFPs from cooking resulted in nervous responses by the human brain (Amouei Torkmahalleh et al., 2022).

Polycyclic aromatic hydrocarbons (PAHs) are organic compounds, which are typical constituents of cigarette smoke and motor-vehicle exhaust. In addition, PAHs are produced from incomplete combustion of organic material and cooking. Polycyclic aromatic hydrocarbons may bind to PM mass, resulting in the formation of particle-bound PAHs (Holme et al., 2019). The concentrations of indoor particle-bound PAHs depend on the distribution of the emission sources, ventilation, and seasonal differences. Based on measurements performed in indoor microenvironments, the highest concentrations of PM-bound PAHs ranged from 550 ng/m^3 to 39000 ng/m^3, were observed in Chinese kitchens, fire stations, and ships (Strandberg et al., 2020). Chemical analysis of the indoor environments in Central India showed that burning of mosquito coil and incense might be as harmful as burning of fuel (coal, kerosene and biomass) due to the high amounts of PAHs released from the burning of mosquito coil (in the range of 66–103 ng/m^3) and incense (4089–14047 ng/m^3) (Verma et al., 2016). Analysis of $PM_{2.5}$ produced from different methods of cooking showed that elevated concentrations of PAHs were produced from deep-frying cooking (36.5 ng/m^3) (See and Balasubramanian, 2008). Furthermore, experimental studies and numerical simulations showed that workers in the bakery and neighboring sales areas have potential health risks from exposure to high levels of PAHs in ambient air (Ielpo et al., 2018). According to the study performed on exposure to combustion byproducts in rural China, the concentration of PAHs in the human venous blood may reach up to 762 ng/mL (Naufal et al., 2010).

The recent studies, performed by Cho et al. (2020) and Edwards et al. (2010) investigated the impact of PAHs on the progression of neurodegenerative diseases in adults and children with prenatal exposure. Among PAHs, the EPA designates 16 high priority pollutants including phenanthrene and benzo[a]pyrene (B[a]P). The effect of B[a]P on the neurobehavioral functions of coke oven workers was also studied in Taiyuan, China (Niu et al., 2010). The authors reported a decline in neurobehavioral function, decreased levels of signal transmitters in the CNS and reduced levels of aminoacid neurotransmitters in coke oven workers with exposure to B[a]P. According to the *in-vivo* studies, performed by Gao et al. (2015), the chronic exposure to B[a]P resulted in the decreases in the cognitive behavior, memory ability, and locomotor activity of the fishes, associated with the increased concentrations of $A\beta_{42}$ peptides observed in their brains.

Alzheimer's Disease (AD) is one of the origins of dementia, with high risk factors among elderly people. According to recent reports, the progression of AD is hypothesized to be associated with the aggregation of amyloid-β (Aβ) peptides into toxic oligomers in the human brain and aggregation of tau proteins into neurofibrillary tangles (Mandelkow and Mandelkow, 2012; Tolar et al., 2020). Literature suggests that Aβ oligomers may cause the development of AD in several pathways, such as destroying neurons, damaging electrochemical signals, harming the respiratory chain due to accumulation in mitochondria, and leading to indirect oxidative stress and detrimental effects on neurons (Kepp, 2012; Sharma and Kim, 2021).

Among different isoforms of Aβ peptide with the number of aminoacids varying from 39 to 43 residues, $A\beta_{42}$ peptide, with 42 aminoacids in its structure, is more abundant in human cerebrospinal fluid (Hamley, 2012). Moreover, in comparison to $A\beta_{40}$, $A\beta_{42}$ peptides are considered to have higher toxicity due to its faster aggregation rate and formation of beta-sheets, resulting from the presence of two additional hydrophobic residues at C-terminus (Hamley, 2012; Kepp, 2012; Jokar et al., 2020). The core sections of $A\beta_{42}$ peptide consist of hydrophilic N-terminus ($A\beta_{1–16}$), central hydrophobic region ($A\beta_{17–21}$), turn ($A\beta_{22–29}$), and hydrophobic C-terminus ($A\beta_{30–42}$) regions (Chakraborty and Das, 2017; Murray et al., 2017). While *in-vitro* studies showed that oligomers mainly consist of extended coils or beta sheets, computational studies also indicated the presence of an antiparallel beta-turn-beta region in their secondary structure (Chen et al., 2017). The change from alpha-helix to beta-sheets is considered as an initial step towards the formation of toxic oligomers (Jokar et al., 2020). The main driving forces that stabilize peptide aggregates are hydrophobic effects and formation of salt bridges (Berhanu and Hansmann, 2012). Although hydrophobic region, C-terminus and turn regions can participate in the initiation of the nucleation of Aβ peptide aggregates, $A\beta_{13–16}$ region of N-terminus is important in the context of oligomerization. Moreover, according to literature, the oligomerization might be promoted with the stabilization of $A\beta_{24–27}$ turn region (Jokar et al., 2020).

Small molecules showed high stability in biological fluids, and might participate in biochemical processes by binding to peptides (Young et al., 2017). Recent in-vitro experiments performed by Wallin et al. (2017), showed that among different cigarette smoke components, PAHs, including phenanthrene, pyrene, and B[a]P increased the aggregation kinetics of Aβ peptide. While *in-vivo* and *in-vitro* experiments showed the enhanced aggregation of Aβ peptides and formation of oligomers in the presence of PAHs (Wallin et al., 2017; Liu et al., 2020), the

molecular interactions between Aβ peptides and PAHs are obscure. In this study, we performed molecular dynamics simulations to investigate the effect of PAH, as one of the major compounds of cooking particles on the structure of $A\beta_{42}$ peptide. B[a]P and phenanthrene are the typical PAHs chosen in our study, which have different number of aromatic rings, different size and hydrophobicity, whereas nicotine was particularly chosen as it is a cigarette smoke component, which is relatively more hydrophilic and has higher tendency to engage in salt bridges and hydrogen bonds.

2 Methodology

2.1 Forcefield validation and structures of molecules

Gromacs 2019.6 software with gromos54a7 forcefield parameters were used to perform atomistic molecular dynamics (MD) simulations (Abraham et al., 2019). Gromos54a7 forcefield was chosen based on the validations provided in literature (Gerben et al., 2014). The optimized geometry and topology parameters of B[a]P, nicotine, and phenanthrene molecule were generated from the Automated Topology Builder (ATB) and Repository server (Version 3.0) (Malde et al., 2011). The forcefield parameters were chosen based on the validation of the densities of B[a]P ($C_{20}H_{12}$), nicotine ($C_{10}H_{14}N_2$) and phenanthrene ($C_{14}H_{10}$) molecules, shown in Table S1. The structures of the molecules are shown in Fig. S1. The coordinates of $A\beta_{42}$ peptide structure were taken from the Protein Data Bank (PDB ID: 1Z0Q (Tomaselli et al., 2006)) with the aminoacid sequence of ^{1}DAEFRHDSGY^{11}EVHHQKLVFF^{21}AEDVGSNKGA^{31}IIGLMVGGVV^{41}IA (total charge of −2).

2.2 Molecular dynamics simulations

A 7 nm × 7 nm × 7 nm box was used to simulate systems with a single $A\beta_{42}$ peptide, in the presence of one B[a]P, one nicotine or one phenanthrene molecule, with the distance between center of masses of organic pollutants and peptide of 2 nm in the beginning of the molecular dynamics run. In addition, to neutralize the negatively charged peptide and to bring physiological conditions, NaCl salt with 0.15 mol/L concentration was included in the systems under the study. SPC water model was used for the solvation. It should be noted, that in order to obtain statistically significant results within the limitations of the simulation box size and computational time, high concentrations of $A\beta_{42}$ peptide, and organic pollutants were used for the simulations, as compared to the concentrations found in the human blood or to the concentrations used for *in-vivo* studies (Gao et al., 2015). The number of molecules inserted in the simulation boxes are shown in Table 1.

The energy minimization step with 100 kJ × mol^{-1} × nm^{-1} of a maximum force constraint was performed. The dynamic runs were performed with an integration time step of 0.002 ps. NVT equilibration was performed for 0.025 ns at temperature of 298 K, followed by NPT equilibration step performed for 0.1 ns at the specified conditions of P = 1 bar and T = 298 K. V-rescale thermostat and Parrinello-Rahman barostat were used for temperature and pressure couplings, respectively. Finally, a long production run of 200 ns was generated, considering that the systems reached equilibrium. However, the simulation was prolonged for additional 100 ns in the system with phenanthrene molecule, as the equilibrium was not reached in 200 ns. LINCS algorithm (Hess et al., 1997) was applied for all bond constraints and periodic boundary conditions were used in *xyz*-directions.

2.3 Analysis of the MD simulations

Visual molecular dynamics (VMD) program was used for the visualization of the simulated systems (Humphrey et al., 1996). The change in the structure of $A\beta_{42}$ peptide from the simulations were studied by determining the solvent accessible surface area (SASA), average radius of gyration (RoG), root mean square (RMS) deviations, and secondary structure of the peptide. Root mean square fluctuations (RMSF) analyses were performed to investigate the change in the positions of C-alpha atoms of the aminoacid residues. The interactions of environmental pollutants and peptide were studied by analyzing the intermolecular distance, and formation of clusters. For the cluster analyses, 0.35 nm distance was defined as a maximum distance between the center of masses of the species to be considered as a cluster. Hydrogen bonds observed between peptide residues and environmental pollutants were identified via VMD software, setting the donor–acceptor distance of 0.30 nm and angle-cutoff distance as 20º. Energy analyses were performed to

Table 1 Number of molecules in the simulated systems of one $A\beta_{42}$ peptide and one PAH

System	$A\beta_{42}$	B[a]P	nicotine	phenanthrene	H_2O	Na^+	Cl^-
$A\beta_{42}$	1	0	0	0	10982	33	31
$A\beta_{42}$ + B[a]P	1	1	0	0	10969	33	31
$A\beta_{42}$ + nicotine	1	0	1	0	10984	33	31
$A\beta_{42}$ + phenanthrene	1	0	0	1	10972	33	31

investigate the strengths interactions between different energy groups.

3 Results and discussion

The cluster and intermolecular distance analyses were performed to investigate the molecular interactions and possible binding of benzo[a]pyrene (B[a]P), nicotine, and phenanthrene molecules with $A\beta_{42}$ monomer occurred within 200 ns of the simulation (Fig. 1).

The formation of a cluster was defined when the maximum distance between center of masses of the residues was 0.70 nm. The formation of a "stable cluster" of $A\beta_{42}$ peptide and environmental pollutants was defined if one cluster remained for 50 ns of the MD simulation. According to Fig. 1A, a stable single cluster of $A\beta_{42}$ peptide monomer and a nicotine molecule was formed within 40 ns of the simulation, indicating the strong binding affinity between nicotine and peptide monomer. The high stability of the peptide-nicotine cluster is a result of the H-bonding observed between peptide and the nicotine molecule. In particular, H-bonds were formed between $A\beta_{42}$ peptide residues, GLN-15 and LYS-16, serving as H-bond donors, and nitrogen atoms of nicotine molecule, serving as H-bond acceptors. In contrast, H-bonds were not observed between $A\beta_{42}$ peptide and B[a]P or phenanthrene molecules, as they do not have H-bond acceptors in their structures. Thus, more time was required for the formation of stable clusters of peptide – B[a]P (125 ns) and peptide – phenanthrene (140 ns).

The obtained results were in good agreement with the intermolecular distances observed between the center of masses of the peptide monomer and B[a]P, nicotine, and phenanthrene molecules (Fig. 1B). As shown in Fig. 1B, minimum intermolecular distance of ~0.5 nm between $A\beta_{42}$ monomer and B[a]P, nicotine and phenanthrene was reached in 90 ns, 40 ns and 140 ns of MD run, respectively. The results also illustrated that B[a]P–$A\beta_{42}$ peptide cluster was more stable, than phenanthrene-$A\beta_{42}$ cluster. The maximum distance value of ~1 nm at 80 ns were observed for the distance between $A\beta_{42}$ peptide and B[a]P, while phenanthrene – $A\beta_{42}$ peptide distance deviated more significantly within the simulation time (with the intermolecular distance of ~4 nm at 45 ns, 70 ns, 110 ns and 140 ns). The literature also showed that different hydrophobicity of PAHs had an impact on the biophysical behavior of B[a]P and phenanthrene (de Gelder et al., 2018). Moreover, B[a]P has five aromatic rings and possess higher hydrophobicity (octanol/water partitioncoefficientlogK_{ow}=6.13),incomparisontophenanthrene molecule, with three aromatic rings (logK_{ow}= 4.46). As the binding of aromatic compounds to Aβ peptide occurs through π-π interactions (Aitken et al., 2003), a stronger binding affinity was observed between the peptide monomer and B[a]P molecule.

Furthermore, to investigate the effect of B[a]P, nicotine, and phenanthrene molecules on the changes in the secondary structure of $A\beta_{42}$ peptide during the simulations, the composition of the secondary structure of the peptide monomer was analyzed (Fig. 2). In addition, the percentage composition of the secondary structure of $A\beta_{42}$ peptide monomers was determined based on the average values of the last 20 ns of the simulations (Table 2).

According to Fig. 2A, large amounts of coil and α-helix regions were observed in the secondary structure of the peptide monomer in the system with no environmental pollutants at the beginning of the simulation. Furthermore, the helix region of $A\beta_{30–34}$ was converted to turns within simulation time. In addition, in the absence of environmental pollutants, inconsequential amounts of β-sheets and β-bridges were observed during the simulation in $A\beta_{33–40}$ and $A\beta_{7–8}$ regions, which were later converted to bends.

In comparison, according to Fig. 2B, in the presence of B[a]P molecule, the formation of β-sheets and β-bridges was observed in $A\beta_{30–33}$ and $A\beta_{39–41}$ segments of the peptide monomer. In addition, the amount of coil (in N- and C-terminuses), 3-Helix ($A\beta_{26–28}$), bend ($A\beta_{8–11}$, $A\beta_{21–23}$) and turn ($A\beta_{32–35}$) structures increased after 120 ns

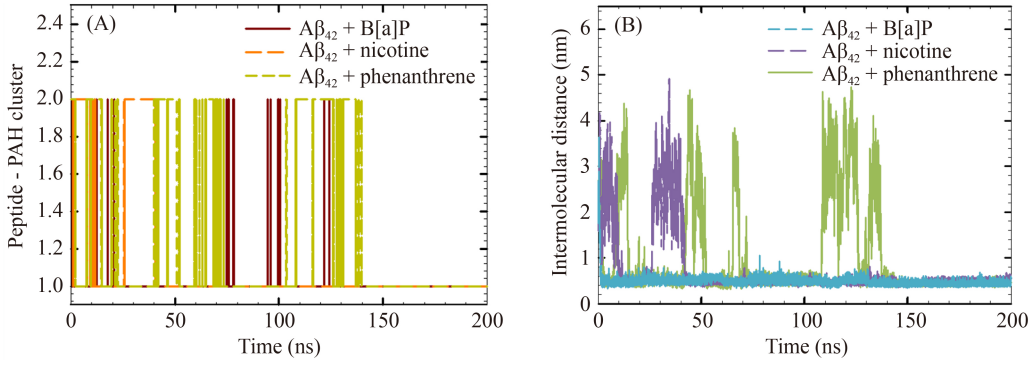

Fig. 1 (A) Formation of clusters of $A\beta_{42}$ monomer with B[a]P, nicotine and phenanthrene molecules, (B) change of the distances between center of masses of $A\beta_{42}$ monomer and B[a]P, nicotine and phenanthrene molecules within the simulation time.

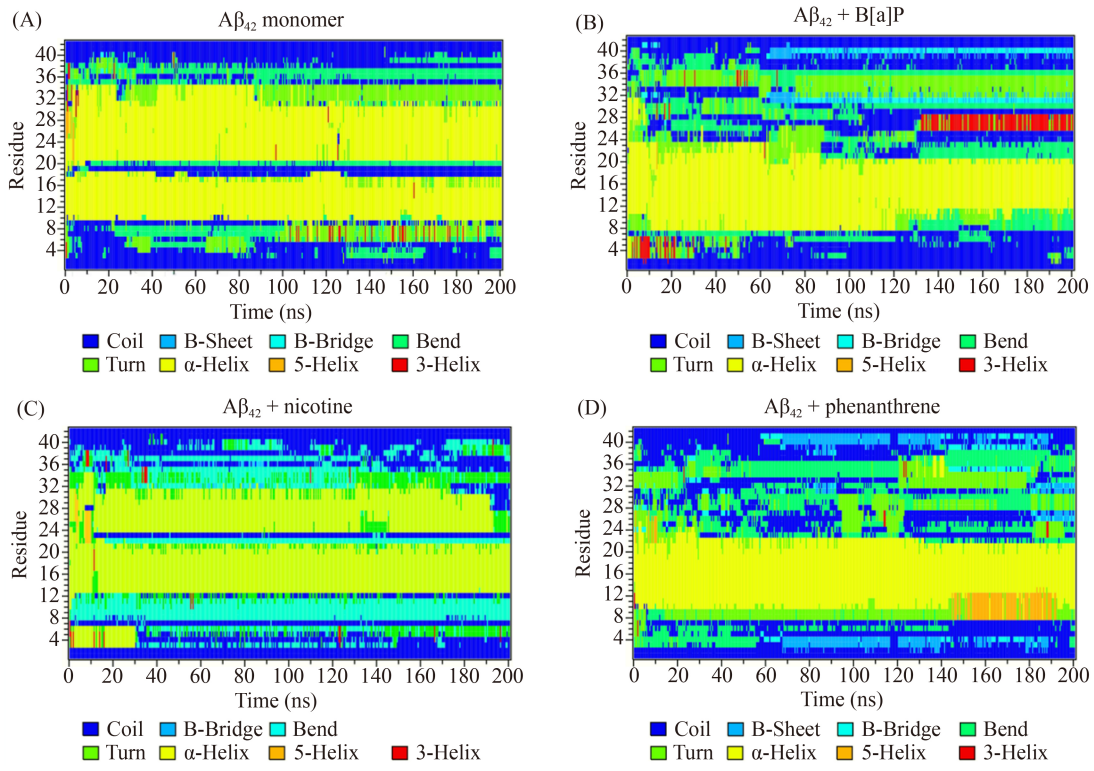

Fig. 2 Time-evolution of secondary structure of $A\beta_{42}$ monomer: (A) in the system with no pollutants, (B) in the presence of one B[a]P molecule, (C) in the presence of one nicotine molecule, (D) in the presence of phenanthrene molecule.

Table 2 Secondary structure of $A\beta_{42}$ peptide monomer in the systems under the study, averaged among last 20 ns of the molecular dynamics run

System	Coil	β-Sheet	β-Bridge	Bend	Turn	α-Helix	3- and 5-Helixes
$A\beta_{42}$	0.29	0	0	0.14	0.14	0.42	0.01
$A\beta_{42}$ + B[a]P	0.33	0.02	0.04	0.21	0.13	0.21	0.06
$A\beta_{42}$ + nicotine	0.34	0	0	0.19	0.16	0.31	0
$A\beta_{42}$ + phenanthrene	0.28	0.1	0.02	0.15	0.17	0.23	0.05

of the MD simulation, after the formation of Aβ monomer-B[a]P cluster. In the presence of nicotine molecule, no β-sheets were observed in the secondary structure of the peptide monomer (Fig. 2C). During MD simulation, a significant amount of α-helix was observed in $A\beta_{13–20}$ and $A\beta_{24–31}$ regions, while coil, bend and turn structures were mainly noticed in the terminuses of the peptide monomer. In complete contrast, in the presence of phenanthrene molecule, noticeable amounts of β-sheets and β-bridge were observed in $A\beta_{2–4}$ and $A\beta_{38–41}$ regions after 70 ns of the simulation run (Fig. 2D). In addition, a beta-turn-beta region was noticed in $A\beta_{26–32}$ segment at 180–200 ns. During the simulation, α-helix region was observed in $A\beta_{10–22}$ segment, while 5-Helix was produced in $A\beta_{7–13}$ after 140 ns of the MD run, when Aβ monomer-phenanthrene cluster was produced.

Overall, according to Fig. 2 and Table 2, B[a]P, nicotine and phenanthrene molecules had a significant effect on the secondary structure of $A\beta_{42}$ monomer. The analysis of the secondary structure of $A\beta_{42}$ monomer showed that in the last 20 ns of the simulations, the amounts of α-helix region decreased in the presence of environmental pollutants. In particular, 21 %, 30 % and 23 % of α-helix were observed in the presence of B[a]P, nicotine and phenanthrene, respectively, in comparison to the system with no environmental pollutants with 42% of α-helix (Table 2). Moreover, according to Table 2, in the presence of the pollutants, $A\beta_{42}$ peptide showed a high tendency to form turn, coil and β-sheet regions instead of alpha-helixes, which would indicate that these molecules might contribute to the progression of AD. Representative snapshots of the structures and binding of $A\beta_{42}$ peptide, B[a]P, nicotine and phenanthrene molecules, visualized via VMD, are shown in Fig. 3.

The visualization of the systems under the study illustrated that initial structure of $A\beta_{42}$ monomer was consisted of helix, turn, bend and coil structures (Fig. 3A). In the end of the molecular dynamics simulation, no beta-sheets

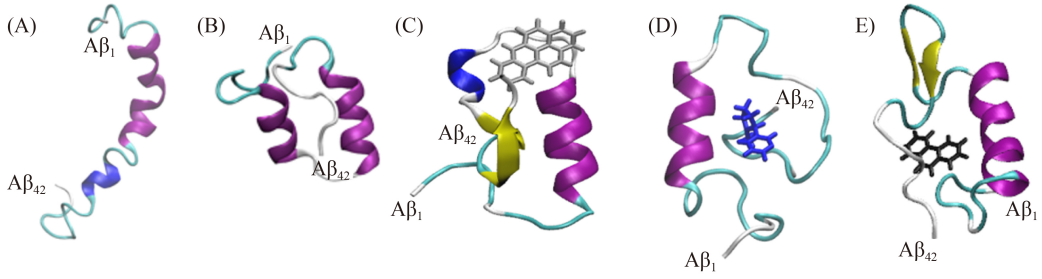

Fig. 3 Representative snapshots of the systems under the study (water molecules and ions are not shown) with indicated $A\beta_1$ of N-terminus and $A\beta_{42}$ of C-terminus of: (A) $A\beta_{42}$ monomer in the beginning of the simulations, (B) $A\beta_{42}$ monomer in the end of 200 ns of the simulation in the absence of environmental pollutants, (C) $A\beta_{42}$ monomer and B[a]P molecule in the end of molecular dynamics (MD) run, (D) $A\beta_{42}$ monomer and nicotine molecule in the end of MD run, (E) $A\beta_{42}$ monomer and phenanthrene molecule in the end of MD run. VMD coloring methods: 1. Secondary structure of peptide: beta sheet = yellow, bridge-beta = tan, alpha helix = purple, 3–10_Helix = blue, bend = cyan, turn = cyan, coil = white. 2. B[a]P molecule – grey, nicotine – blue, phenanthrene – black.

were observed in the structure of $A\beta_{42}$ monomer in the absence of the environmental pollutants (Fig. 3B). In comparison, according to Fig. 3C, in the presence of B[a]P molecule, the beta-turn-beta region were formed in $A\beta_{31–40}$ region of the C-terminus in the end of the simulation, consistent with the results of the secondary structure analysis of the peptide (Fig. 2B). According to Fig. 3D, in the presence of nicotine, in the end of the simulation, no β-sheets were observed in the secondary structure of the peptide monomer. In the presence of phenanthrene, in the end of the simulation, the β-sheets were observed in the region of $A\beta_{26–32}$ (Fig. 3E), as was shown previously in Fig. 2D.

The distance analyses between center of masses of the amino acid residues of $A\beta_{42}$ peptide, and B[a]P, nicotine and phenanthrene molecules were further performed for the last 20 ns of the simulations to investigate the binding sites of the peptide monomer and environmental pollutants in the end of the simulations, after the formation of stable clusters (Fig. 4).

According to Fig. 4, in the last 20 ns of the simulation, B[a]P molecule was located closer to the region of $A\beta_{20–30}$ with the aminoacids sequence of F^{21}AEDVG-SNKGA. The smallest distances between the center of masses were observed between B[a]P and GLY-25 (0.45 nm distance), VAL-24 (0.65 nm), SER-26 (0.61 nm), LYS-28 (0.62 nm), GLY-29 (0.72 nm) residues, indicating that B[a]P was bound to this region in the end of the simulation. In addition, based on Fig. 4, the N- and C-terminuses were located at the highest remoteness from the B[a]P molecule (1.7–2.5 nm distance), as was also shown in Fig. 3C. As it was noted from Fig. 2B, B[a]P molecule was bound to coil-turn-coil region ($A\beta_{20–30}$), which was later transformed to bend-coil-helix region after binding of B[a]P. In contrast, according to Fig. 4, in the presence of nicotine and phenanthrene, the $A\beta_{20–30}$ region was located far from the environmental pollutants, while both N- and C- terminus regions of the peptide were located closer to nicotine and phenanthrene molecules. Low distances were observed between nicotine

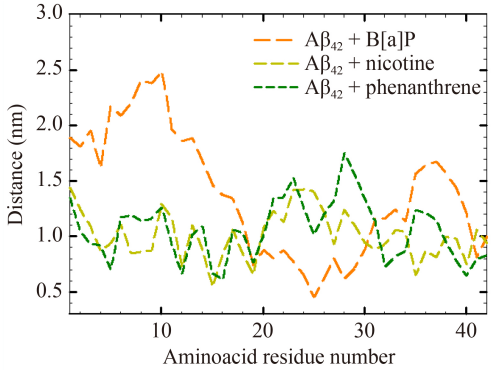

Fig. 4 Distances between center of masses of the amino acid residues of $A\beta_{42}$ monomer and B[a]P, nicotine and phenanthrene molecules averaged within the last 20 ns of the simulations.

and the aminoacid residues with coil and helix structures: VAL-12 (0.72 nm distance), GLN-15 (0.55 nm with H-bonding, as mentioned previously), PHE-19 (0.66 nm) and MET-35 (0.65 nm). For the phenanthrene, the binding site of the peptide monomer at the end of the simulation was observed for the region with the aminoacid residues of helix, ARG-5 (0.70 nm distance), VAL-12 (0.67 nm), GLN-15 (0.66 nm) and coil/β-sheet VAL-40 (0.64 nm). Thus, the equilibrium binding sites for the environmental pollutants were mainly the coil, bend, and helix regions of the peptide monomer. In addition, phenanthrene was located near VAL-40 residue with a high tendency to form β-sheet in that region, as was shown in Fig. 2D.

The time-evolution of the peptide structure due to the binding of B[a]P, nicotine, or phenanthrene molecules were further studied by performing RMS, SASA, and RoG analyses (Fig. 5).

The RMS deviations of the peptide structure were ~1.21 nm at the end the simulation of the system with $A\beta_{42}$ peptide monomer in the absence of environmental pollutants (Fig. 5A). The RMS deviations became slightly lower with the addition of B[a]P after 70 ns of the

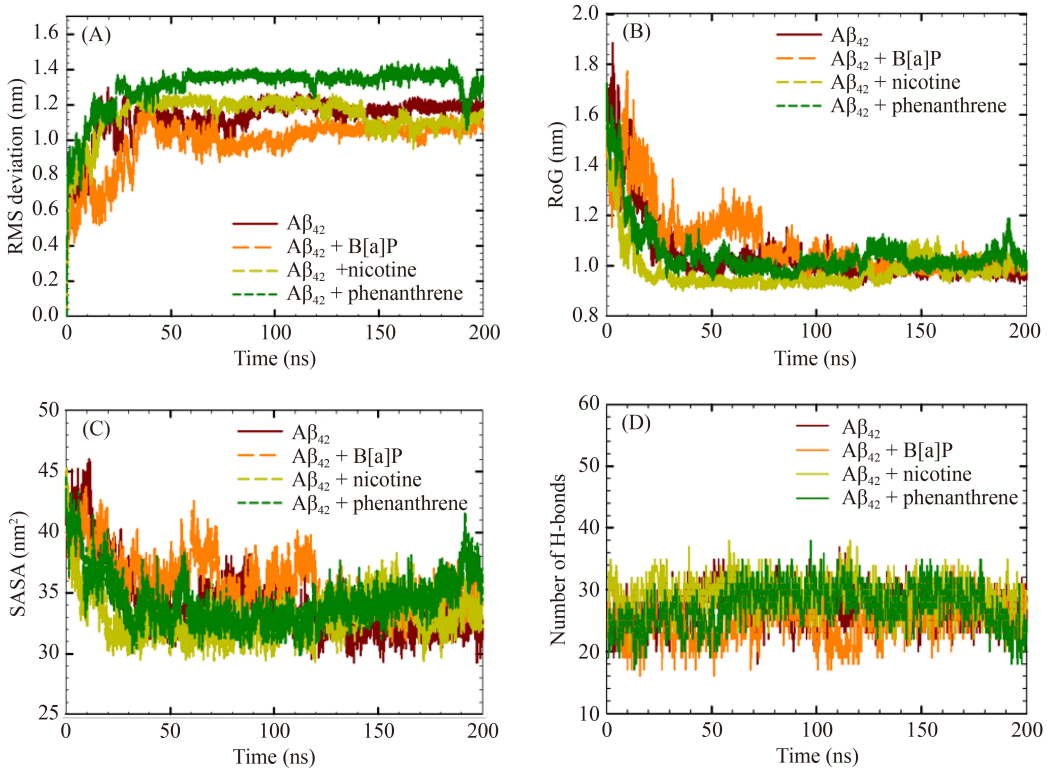

Fig. 5 Time-evolution of (A) root-mean square deviations, (B) radius of gyration, (C) solvent accessible surface area, (D) intrapeptide H-bonds of Aβ$_{42}$ peptide monomer in the systems under study within the simulation time.

simulation (deviations around ~1.08 nm) and nicotine molecule after 150 ns of the MD run (deviations around ~1.13 nm). In comparison, with the addition of phenanthrene, the RMS deviations of the peptides increased up to 1.42 nm, with a sharp decrease to 1.05 nm at ~190 ns of the MD run. Based on Fig. 5B and Fig. 5C, in general, RoG and SASA values of Aβ$_{42}$ peptide did not significantly change during the simulations with the addition of B[a]P and nicotine molecules. Based on the RoG analysis (Fig. 5B), starting from nvt-equilibration step, the radius of Aβ$_{42}$ peptide deviated from ~1.53 nm to ~1 nm within 200 ns of the simulation, indicating that the peptide structure became more compact within the simulated time. The SASA values (Fig. 5C) decreased from ~42 nm^2 to ~34±1 nm^2 within the simulation time in the presence of B[a]P and nicotine molecules. In addition, according to the results of H-bonds analysis (Fig. 5D), average amounts of H-bonds observed within a peptide in the last 20 ns of the simulations were ~27±2, 26±3, 28±3 and 24±3, in the systems without PAH, with B[a]P, nicotine and phenanthrene molecules, respectively.

It should be noted that a sharp decrease in RMS deviations was observed in the last 10 ns of the simulations in the structure of the Aβ$_{42}$ peptide monomer in the presence of phenanthrene molecule (Fig. 5). The decrease in RMS deviations was consistent with sharp increases in SASA and RoG values of the peptide monomer and a decrease in intrapeptide H-bonds over the last 20 ns of the simulation. The investigation of the change in the distances between phenanthrene and aminoacid residues during the last 50 ns of the simulation showed that this phenomenon could occur due to the change in the binding site of phenanthrene and Aβ$_{42}$ monomer (Fig. S2). Particularly, in the last 20 ns of the simulation, phenanthrene became closely located to both N-terminus and C-terminus of the peptide monomer, while getting away from the residues LYS-16 and LEU-34. As it was mentioned, the simulation was prolonged for the system with peptide monomer and phenanthrene, an additional 100 ns run was performed from the last trajectory obtained after the first 200 ns run. To investigate further changes in the structure of the peptide in the presence of phenanthrene, changes in RMS deviations, RoG and secondary structure of the peptide monomer were studied (Fig. S3). The results showed that the RMS deviations were increased from 250 ns to 300 ns of the simulation (Fig. S3A), while the RoG values were decreased at the same time period (Fig. S3B). This observation was also correlated with transformation of the helix structure in the Aβ$_{10-22}$ region to coil and bend structures, and formation of β-sheets in N- and C-terminuses (Fig. S3B). Overall, continuous RMS deviations and changes in the RoG values in the structure of the peptide monomer in the presence of phenanthrene could be determined by the size of the PAH. In comparison to B[a]P with five aromatic rings,

phenanthrene with three aromatic rings interfered with the peptide structure more significantly, leading to the changes in the secondary structure of the peptide monomer.

In addition, the RMSF analyses were further performed to investigate the changes in the fluctuations of the positions of the aminoacid residues of $A\beta_{42}$ peptide structure with the addition of the environmental pollutants in the end of the simulations (Fig. 6).

According to Fig. 6, during the last 20 ns of the simulation, in the system with $A\beta_{42}$ peptide monomer with no environmental pollutants, the highest fluctuations were observed in the position of ASP-1 and ALA-2 residues (RMSF values at ~0.4–0.6 nm). The fluctuations of the other residues were in the range of ~0.05–0.2 nm, which were comparatively lower than the fluctuations in the positions of the aminoacid residues observed in the presence of environmental pollutants. In the presence of B[a]P molecules, enhanced fluctuations were noted in the positions of the amino acids in the region of $A\beta_{20–28}$ (with RMSF values ~0.15–0.35 nm), which was considered as a binding site for B[a]P, as discussed previously. The lowest fluctuations were observed in the region of $A\beta_{30–35}$ (with RMSF values ~0.09–0.10 nm), which were involved in the formation of β-sheets. In contrast, in the end of the simulated time, in the presence of nicotine, elevated RMSF values were observed for the aminoacids for the residues GLY-25, ALA-30, LEU-34 and ILE-41 (with RMSF values ~0.30–0.33 nm). The lowest fluctuations of the aminoacid residues were observed in the region of $A\beta_{12–16}$ (with RMSF values ~0.10–0.12 nm), which was involved in the binding to nicotine molecule. In the presence of phenanthrene molecule, enhanced RMSF values were observed for the aminoacids in the region of $A\beta_{8–10}$ (with RMSF values ~0.30–0.37 nm), $A\beta_{26–32}$ (β-sheets region) and C-terminus (with RMSF values ~0.19–0.50 nm). The lowest fluctuations of the aminoacid residues were observed in the region of $A\beta_{15–20}$ (with RMSF values ~0.12–0.15 nm).

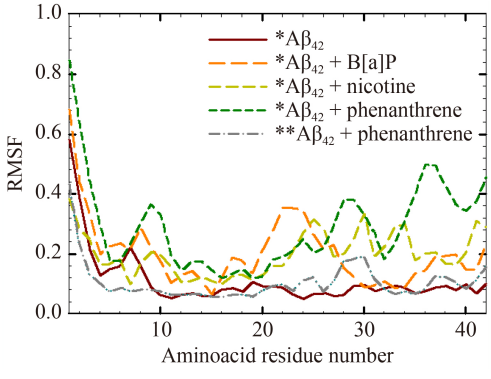

Fig. 6 RMSF of aminoacid residues of $A\beta_{42}$ peptide monomer (*: averaged among last 20 ns of the simulations that was 180–200 ns of the molecular dynamics run, **: in the range of 150–170 ns of the MD run).

Although, high fluctuations were observed in the positions of the residues located on the N-terminus (ASP-1, ALA-2, GLU-3) in all systems under the study, large RMSF values were also observed for the C-terminus in the presence of phenanthrene in the last 20 ns of the simulation. Consistent with the observations from the distance analyses (Fig S2), the small phenanthrene molecule could intercalate with the peptide structure and affect the structure of the peptide, particularly, in the regions of N-terminus and C-terminus, more significantly, in comparison to B[a]P and nicotine molecules, which stabilized $A\beta_{42}$ monomer structure within the simulated time. This observation was consistent with RMSD, SASA and RoG and distance analyses, which showed that among the three environmental pollutants under the study, there could be enhanced interactions of the phenanthrene molecule and the peptide monomer in the last 20 ns of the run. Hence, RMSF analysis was also performed for the period of 150–170 ns of the MD run for the system with phenanthrene molecule. For this period, the fluctuations in the positions of the aminoacid residues were significantly lower, in comparison to the values observed at the end of the simulations with all of the environmental pollutants under the study. This observation indicates that the positions of the aminoacid residues were stable in the presence of phenanthrene at 150–170 ns of the simulation, before the dynamic interactions between phenanthrene and N-terminus and C-terminus of the peptide monomer at 180–200 ns of the simulation.

Furthermore, the energy analyses were performed to investigate the type of the interactions that predominated between the peptide and the environmental pollutants during the last 10 ns of the molecular dynamics runs (Table S2). It should be noted, that Wallin et al. suggested that the initiation of the aggregation might occur due to electrostatic interactions, while the formation of larger oligomers might happen due to hydrophobic forces (Wallin et al., 2017). The results of our study showed that with the addition of the environmental pollutants, short-range coulombic intrapeptide interactions slightly increased, while the van der Waals intrapeptide interactions decreased in the simulated systems. This observation showed that the electrostatic interactions within the peptide increased in the presence of B[a]P, nicotine and phenanthrene molecules, suggesting that peptides might undergo an initiation of the aggregation at the mentioned environments.

In addition, according to the *in-vitro* studies from the literature, Wallin et al. reported that enhanced aggregation kinetics of the peptides were observed in the presence of the PAHs with more than two aromatic rings in their structures (Wallin et al., 2017). Consistent with the observations from our study, B[a]P with five aromatic rings might increase aggregation kinetics of Aβ peptides by making stable clusters with peptides and changing

their secondary structure. Moreover, phenanthrene with three aromatic rings intensively altered the secondary structure of peptides, leading to the enhanced formation of β-sheets, which might also result in the increased aggregation kinetics of the peptides.

4 Conclusions

In our study, the structure of $A\beta_{42}$ peptide monomer was affected by benzo[a]pyrene, nicotine and phenanthrene molecules, depending on their hydrophobicity, size, and H-bonding capacity. Among three organic air pollutants under the study, nicotine made most stable cluster with $A\beta_{42}$ peptide within 40 ns of the MD run due to nicotine's H-bonding capacity. In contrast, phenanthrene molecule, due to its small size, could interfere with the peptide monomer more strongly, leading to high deviations in the radius of gyration (for up to 20 %) in the structure of the peptide in the end of the MD run. Overall, the secondary structure of the peptide monomer was affected by the presence of the organic pollutants with the formation of more turn (higher for up to 20 %), coil (for up to 17 %), bend (for up to 20 %) and β-sheet (for up to 10 %) regions instead of alpha-helixes (reduced to 25 %–50 %), suggesting that benzo[a]pyrene, nicotine, and phenanthrene might have effect on the progression of Alzheimer's Disease. Consequently, further in-depth analysis on the effect of organic pollutants on the oligomerization of Aβ peptides would be necessary to gain further insides into the effect of the air pollution on the neurodegenerative diseases.

Acknowledgements The research was conducted under the project "OPCRP2022003 Exposure to Cooking Ultrafine Particles and Neurodegenerative Disease: Clinical Exposure Studies and Computer Modeling" and "11022021FD2905 Efficient thermal valorization of municipal sewage sludge in fluidized bed systems: Advanced experiments with process modeling".

We thank Dr. Jianguo Li for his valuable support and insightful comments in this work.

Electronic Supplementary Material Supplementary material is available in the online version of this article at https://doi.org/10.1007/s11783-023-1615-2 and is accessible for authorized users.

References

VAbraham M J, Van Der Spoel D, Lindahl E, Hess B (2019). GROMACS User Manual Version 2019. 6

Aitken J F, Loomes K M, Konarkowska B, Cooper G J (2003). Suppression by polycyclic compounds of the conversion of human amylin into insoluble amyloid. Biochemical Journal, 374(3): 779–784

Amouei Torkmahalleh M, Naseri M, Nurzhan S, Gabdrashova R, Bekezhankyzy Z, Gimnkhan A, Malekipirbazari M, Jouzizadeh M, Tabesh M, Farrokhi H, et al. (2022). Human exposure to aerosol from indoor gas stove cooking and the resulting nervous system responses. Indoor Air, 32(2): e12983

Berhanu W M, Hansmann U H (2012). Structure and dynamics of amyloid-β segmental polymorphisms. PLoS One, 7(7): e41479

Calderón-Garcidueñas L (2016). Smoking and cerebral oxidative stress and air pollution: a dreadful equation with particulate matter involved and one more powerful reason not to smoke anything! Journal of Alzheimer's Disease , 54(1): 109–112

Chakraborty S, Das P (2017). Emergence of alternative structures in amyloid beta 1-42 monomeric landscape by n-terminal hexapeptide amyloid inhibitors. Scientific Reports, 7(1): 9941(1:12)

Chen G F, Xu T H, Yan Y, Zhou Y R, Jiang Y, Melcher K, Xu H E (2017). Amyloid beta: structure, biology and structure-based therapeutic development. Acta Pharmacologica Sinica, 38(9): 1205–1235

Cho J, Sohn J, Noh J, Jang H, Kim W, Cho S K, Seo H, Seo G, Lee S K, Noh Y, et al. (2020). Association between exposure to polycyclic aromatic hydrocarbons and brain cortical thinning: the Environmental Pollution-Induced Neurological EFfects (EPINEF) study. Science of the Total Environment, 737: 140097

de Gelder S, Sundh H, Pelgrim T N M, Rasinger J D, van Daal L, Flik G, Berntssen M H G, Klaren P H M (2018). Transepithelial transfer of phenanthrene, but not of benzo[a]pyrene, is inhibited by fatty acids in the proximal intestine of rainbow trout (*Oncorhynchus mykiss*). Comparative Biochemistry and Physiology. Toxicology & Pharmacology: CBP, 204: 97–105

Edwards S C, Jedrychowski W, Butscher M, Camann D, Kieltyka A, Mroz E, Flak E, Li Z, Wang S, Rauh V, Perera F (2010). Prenatal exposure to airborne polycyclic aromatic hydrocarbons and children's intelligence at 5 years of age in a prospective cohort study in Poland. Environmental Health Perspectives, 118(9): 1326–1331

Gao D, Wu M, Wang C, Wang Y, Zuo Z (2015). Chronic exposure to low benzo[a]pyrene level causes neurodegenerative disease-like syndromes in zebrafish (*Danio rerio*). Aquatic Toxicology (Amsterdam, Netherlands), 167: 200–208

Gerben S R, Lemkul J A, Brown A M, Bevan D R (2014). Comparing atomistic molecular mechanics force fields for a difficult target: a case study on the Alzheimer's amyloid β-peptide. Journal of Biomolecular Structure and Dynamics, 32(11): 1817–1832

Hahad O, Lelieveld J, Birklein F, Lieb K, Daiber A, Münzel T (2020). Ambient air pollution increases the risk of cerebrovascular and neuropsychiatric disorders through induction of inflammation and oxidative stress. International Journal of Molecular Sciences, 21(12): 4306

Hamley I W (2012). The amyloid beta peptide: a chemist's perspective. Role in Alzheimer's and fibrillization. Chemical Reviews, 112(10): 5147–5192

Hess B, Bekker H, Berendsen H J C, Fraaije J G E M (1997). LINCS: A linear constraint solver for molecular simulations. Journal of Computational Chemistry, 18(12): 1463–1472

Heusinkveld H J, Wahle T, Campbell A, Westerink R H S, Tran L, Johnston H, Stone V, Cassee F R, Schins R P F (2016). Neurodegenerative and neurological disorders by small inhaled particles. Neurotoxicology, 56: 94–106

Holme J A, Brinchmann B C, Refsnes M, Låg M, Øvrevik J (2019).

Potential role of polycyclic aromatic hydrocarbons as mediators of cardiovascular effects from combustion particles. Environmental Health, 18(1): 74

Humphrey W, Dalke A, Schulten K (1996). VMD: visual molecular dynamics. Journal of Molecular Graphics, 14(1): 33–38, 27–28

Ielpo P, Taurino M R, Buccolieri R, Placentino C M, Gallone F, Ancona V, Di Sabatino S (2018). Polycyclic aromatic hydrocarbons in a bakery indoor air: trends, dynamics, and dispersion. Environmental Science and Pollution Research International, 25(29): 28760–28771

Jokar S, Erfani M, Bavi O, Khazaei S, Sharifzadeh M, Hajiramezanali M, Beiki D, Shamloo A (2020). Design of peptide-based inhibitor agent against amyloid-β aggregation: molecular docking, synthesis and *in vitro* evaluation. Bioorganic Chemistry, 102: 104050

Kepp K P (2012). Bioinorganic chemistry of Alzheimer's disease. Chemical Reviews, 112(10): 5193–5239

Klepeis N E, Nelson W C, Ott W R, Robinson J P, Tsang A M, Switzer P, Behar J V, Hern S C, Engelmann W H (2001). The national human activity pattern survey (NHAPS): a resource for assessing exposure to environmental pollutants. Journal of Biomolecular Structure and Dynamics, 11(3): 231–252

Kwon H S, Ryu M H, Carlsten C (2020). Ultrafine particles: unique physicochemical properties relevant to health and disease. Experimental & Molecular Medicine, 52(3): 318–328

Liu D, Zhao Y, Qi Y, Gao Y, Tu D, Wang Y, Gao H M, Zhou H (2020). Benzo(a)pyrene exposure induced neuronal loss, plaque deposition, and cognitive decline in APP/PS1 mice. Journal of Neuroinflammation, 17(1): 258

Malde A K, Zuo L, Breeze M, Stroet M, Poger D, Nair P C, Oostenbrink C, Mark A E (2011). An Automated force field Topology Builder (ATB) and repository: version 1.0. Journal of Chemical Theory and Computation, 7(12): 4026–4037

Mandelkow E M, Mandelkow E (2012). Biochemistry and cell biology of tau protein in neurofibrillary degeneration. Cold Spring Harbor Perspectives in Medicine, 2(7): a006247

Murray B, Sharma B, Belfort G (2017). N-terminal hypothesis for Alzheimer's disease. ACS Chemical Neuroscience, 8(3): 432–434

Naufal Z, Zhiwen L, Zhu L, Zhou G D, McDonald T, He L Y, Mitchell L, Ren A, Zhu H, Finnell R, Donnelly K C (2010). Biomarkers of exposure to combustion by-products in a human population in Shanxi, China. Journal of Exposure Science & Environmental Epidemiology, 20(4): 310–319

Niu Q, Zhang H, Li X, Li M (2010). Benzo[a]pyrene-induced neurobehavioral function and neurotransmitter alterations in coke oven workers. Occupational and Environmental Medicine, 67(7): 444–448

Oberdörster G, Sharp Z, Atudorei V, Elder A, Gelein R, Kreyling W, Cox C (2004). Translocation of inhaled ultrafine particles to the brain. Inhalation Toxicology, 16(6–7): 437–445

See S W, Balasubramanian R (2008). Chemical characteristics of fine particles emitted from different gas cooking methods. Atmospheric Environment, 42(39): 8852–8862

Shang K, Chen Z, Liu Z, Song L, Zheng W, Yang B, Liu S, Yin L (2021). Haze prediction model using deep recurrent neural network. Atmosphere (Basel), 12(12): 1625

Sharma C, Kim S R (2021). Linking oxidative stress and proteinopathy in Alzheimer's disease. Antioxidants(Basel), 10(8): 1231

Strandberg B, Österman C, Koca Akdeva H, Moldanová J, Langer S (2020). The use of polyurethane foam (PUF) passive air samplers in exposure studies to PAHs in Swedish seafarers. Polycyclic Aromatic Compounds, 42(2): 448–459

Tolar M, Abushakra S, Sabbagh M (2020). The path forward in Alzheimer's disease therapeutics: reevaluating the amyloid cascade hypothesis. Alzheimers Dement, 16(11): 1553–1560

Tomaselli S, Esposito V, Vangone P, van Nuland N A, Bonvin A M J J, Guerrini R, Tancredi T, Temussi P A, Picone D (2006). The alpha-to-beta conformational transition of Alzheimer's Abeta-(1–42) peptide in aqueous media is reversible: a step by step conformational analysis suggests the location of beta conformation seeding. Chembiochem, 7(2): 257–267

Verma R, Patel K S, Verma S K (2016). Indoor polycyclic aromatic hydrocarbon concentration in Central India. Polycyclic Aromatic Compounds, 36(2): 152–168

Wallin C, Sholts S B, Österlund N, Luo J, Jarvet J, Roos P M, Ilag L, Gräslund A, Wärmländer S K T S (2017). Alzheimer's disease and cigarette smoke components: effects of nicotine, PAHs, and Cd(II), Cr(III), Pb(II), Pb(IV) ions on amyloid-β peptide aggregation. Scientific Reports, 7(1): 14423(1-14)

Young L M, Ashcroft A E, Radford S E (2017). Small molecule probes of protein aggregation. Current Opinion in Chemical Biology, 39: 90–99

Zhang Z, Tian J, Huang W, Yin L, Zheng W, Liu S (2021). A haze prediction method based on one-dimensional convolutional neural network. Atmosphere (Basel), 12(10): 1327